Collisional Properties of *p*-Wave Feshbach Molecules

Yasuhisa Inada,[1,2] Munekazu Horikoshi,[1] Shuta Nakajima,[1,3] Makoto Kuwata-Gonokami,[1,2]
Masahito Ueda,[1,3] and Takashi Mukaiyama[1]

[1]*ERATO Macroscopic Quantum Control Project, JST, Yayoi, Bunkyo-Ku, Tokyo 113-8656, Japan*
[2]*Department of Applied Physics, University of Tokyo, Hongo, Bunkyo-Ku, Tokyo 113-8656, Japan*
[3]*Department of Physics, University of Tokyo, Hongo, Bunkyo-ku, Tokyo 113-0033, Japan*
(Received 10 March 2008; published 3 September 2008; publisher error corrected 16 September 2008)

We have observed *p*-wave Feshbach molecules for all three combinations of the two lowest hyperfine spin states of ^{6}Li. By creating a pure molecular sample in an optical trap, we measured the inelastic collision rates of *p*-wave molecules. We have also measured the elastic collision rate from the thermalization rate of a breathing mode which was excited spontaneously upon molecular formation.

Ultracold atomic gases with tunable interaction via a Feshbach resonance have opened up possibilities for studying a variety of novel phenomena in quantum degenerate phases. In particular, *s*-wave Feshbach resonances have been widely used to study the crossover between Bose-Einstein condensation (BEC) and Bardeen-Cooper-Schrieffer (BCS) superfluidity [1–6]. One of the greatest challenges in the field of trapped Fermi gases is the realization of superfluidity with pairs of atoms in a nonzero relative orbital angular momentum state [7–9]. In such systems, a rich variety of phases are expected to emerge due to complex order parameters [10–14]. Non-*s*-wave superfluidity has so far been realized in superfluid ^{3}He [15], strontium ruthenate superconductors [16], and high-T_c copper-oxide superconductors.

Until now, ^{40}K and ^{6}Li have been utilized to study *p*-wave Feshbach resonances [17–24]. The locations of *p*-wave Feshbach resonances of ^{6}Li have been accurately determined by Zhang *et al.* [17] and Schunck *et al.* [18]. Zhang *et al.* detected the formation of *p*-wave molecules of ^{6}Li in one of the three combinations of the two lowest hyperfine spin states, $|F = 1/2, m_F = 1/2 \rangle$ ($\equiv |1\rangle$) and $|F = 1/2, m_F = -1/2 \rangle$ ($\equiv |2\rangle$), but molecules were not detected in the $|1\rangle - |1\rangle$ state, which is the most promising candidate for a *p*-wave condensate. Recently, Fuchs *et al.* measured the binding energies and molecular magnetic moments of ^{6}Li *p*-wave molecules [19]. Gaebler *et al.* detected *p*-wave Feshbach molecules of ^{40}K through the anisotropic energy release at the dissociation [20,21]. The lifetime of ^{40}K molecules were found to be less than 10 ms, even on the BEC side of the resonance due to dipolar relaxation [21].

While *s*-wave Feshbach molecules are highly stable against vibrational quenching near a Feshbach resonance, it is not known to what extend *p*-wave molecules suffer from inelastic collisions. Therefore, studying collisional properties of *p*-wave Feshbach molecules is an important step toward realization of *p*-wave molecular condensates. In this Letter, we present elastic and inelastic collisional

properties of ^{6}Li$_2$ *p*-wave Feshbach molecules. To suppress the loss of molecules due to atom-dimer collisions, we blew away residual atoms by irradiating a resonant light pulse immediately after the molecules were created [25–27]. The resultant pure molecular sample in an optical trap enabled us to measure the inelastic decay rates of molecules precisely. We measured the atom-dimer and dimer-dimer inelastic collision coefficients from the decay of molecules. We also measured the dimer-dimer elastic collision rate from the thermalization time of breathing-mode oscillations of the cloud which were spontaneously excited after the creation of molecules.

Our experiments were performed using a quantum degenerate gas of ^{6}Li in the $|1\rangle$ and $|2\rangle$ spin states. We evaporated the atoms in a crossed beam optical dipole trap at 300 G, where the elastic collision cross section between $|1\rangle$ and $|2\rangle$ takes on a local maximum. After evaporation for 4 s, a mixture of 5×10^5 atoms in $|1\rangle$ and $|2\rangle$ with equal population and the temperature of $T/T_F \sim 0.25$ was prepared. The trap frequencies (ω_x, ω_y, ω_z) in the *x*, *y* (horizontal) and *z* (vertical) directions at the final trap depth are $2\pi \times (39, 760, 780)$ Hz. By stabilizing the currents in the Feshbach coils, we suppressed magnetic-field fluctuations due to current noise down to 10 mG.

To create $|1\rangle - |1\rangle$ molecules, we first ramp the magnetic field up to the Feshbach resonance of $|2\rangle - |2\rangle$ at 215 G to eliminate atoms in the $|2\rangle$ state. After preparing the atoms in the pure $|1\rangle$ state, we create molecules by ramping the magnetic field to a value near the Feshbach resonance of the $|1\rangle - |1\rangle$ state at $B_0 = 158.5(7)$ G. Because of the small shift of $m_l = \pm 1$ and $m_l = 0$ resonances [22], we were unable to select a specific m_l state. The time sequence for creating $|1\rangle - |1\rangle$ molecules is shown in Fig. 1(a). When the magnetic field reached the resonance, the sample was irradiated with a 25 μs pulse of resonant light ("blast") to remove unpaired atoms from the trap. Molecules are relatively immune to the blast light due to the small Franck-Condon factor for the optical transi-
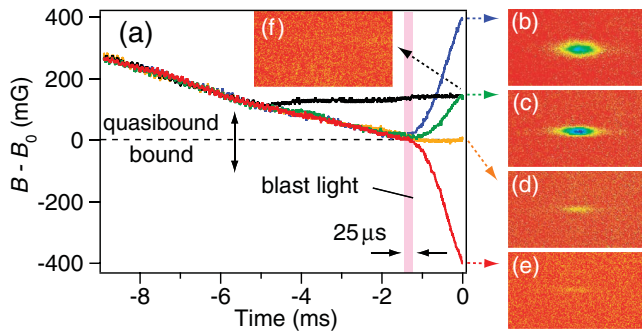
FIG. 1 (color). (a) Time sequence of magnetic field to create molecules. Magnetic field is ramped adiabatically from above toward the Feshbach resonance ($B = B_0$). (b),(c) Absorption images of dissociated molecules for an upward magnetic field ramp. (d),(e) Atoms in a molecular gas detected at (d) or below (e) the resonance. (f) No atoms and molecules are detected when the magnetic field stays far off resonance.
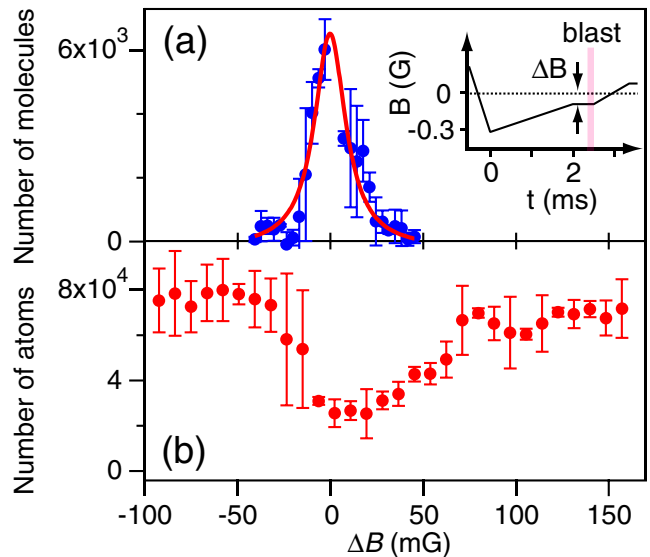

FIG. 2 (color online). (a) Number of $|1\rangle - |1\rangle$ molecules created as a function of magnetic-field detuning ΔB. The solid curve shows a Lorentzian fit to the data. Inset shows the time sequence of magnetic field for data taking. (b) Number of atoms remaining after a hold time of 25 ms as a function of ΔB.

tion. After blasting the atoms, the magnetic field was ramped up above the resonance [Figs. 1(b) and 1(c)], kept at the resonance [Fig. 1(d)], or ramped down below the resonance [Fig. 1(e)] before taking absorption images. The blue, green, orange, and red curves in Fig. 1(a) correspond to the magnetic-field sequence for the images in Figs. 1(b)–1(e), respectively. Ramping the magnetic field to a value above the resonance, as shown by the blue and green curves, allows us to clearly image the dissociated atoms. As shown by the orange and red curves, the atoms in bound molecules are detected, albeit weakly, because of a finite Franck-Condon factor for the optical transition. When the magnetic field is kept away from the resonance by $\Delta B = +100$ mG, no atoms were detected [Fig. 1(f)], indicating the blast light had almost completely removed the unpaired atoms [28]. Therefore, the atoms imaged in Figs. 1(d) and 1(e) are not unpaired atoms but those forming molecules. As seen in Figs. 1(b)–1(d), the higher magnetic field was applied for dissociation, the more widely the cloud expanded during the same time of flight of 500 μs. This indicates that faster ramping of the magnetic field leads to higher dissociation energy. We produced $|1\rangle - |2\rangle$ and $|2\rangle - |2\rangle$ molecules in a similar manner by using Feshbach resonances at 184.9(7) G and 214.5(6) G, respectively.

To investigate the range of magnetic field over which molecules can be formed efficiently, we ramped the magnetic field from below up to the resonance. This eliminates the possibility of adiabatic molecular formation. As shown in the inset of Fig. 2(a), we first ramped down the field across the resonance at a fast rate in order to minimize the atomic loss. We then swept the magnetic field in 2 ms to a value at which the number of molecules was measured. After the molecular formation during a hold time of 500 μs, the blast light was turned on to remove unpaired atoms. Figure 2(a) shows the number of molecules vs magnetic-field detuning ΔB, where ΔB is positive when the magnetic field is higher than the resonance and its

origin $\Delta B = 0$ is defined as the magnetic field at which the maximum number of molecules are created. At the peak, 15% of atoms are converted to molecules, which is consistent with previous experiments [17,20]. Figure 2(b) shows the atomic loss measured after the 25-ms hold time for each magnetic field. An asymmetry in the loss feature is clearly seen, as observed by other groups [18,19]. Note that the valley of the loss curve shifts from the peak of the molecular creation curve. The origin of the shift is unclear and merits further study.

In the process of creating molecules, breathing oscillations were excited spontaneously. This is because the molecules were created over the entire cloud of the Fermi-degenerate atoms, which is larger than the equilibrium cloud size of molecules [29]. Figure 3 shows the time evolution of $T^*(t)$, defined by $T^*(t) = m\omega_x^2 \sigma_x^2(t)/k_B$, where m is the mass of molecules and σ_x is the root-mean-square radius of the molecular cloud in the x direction. The size of the molecular cloud is largest when the molecules are created. The frequency of initial oscillations
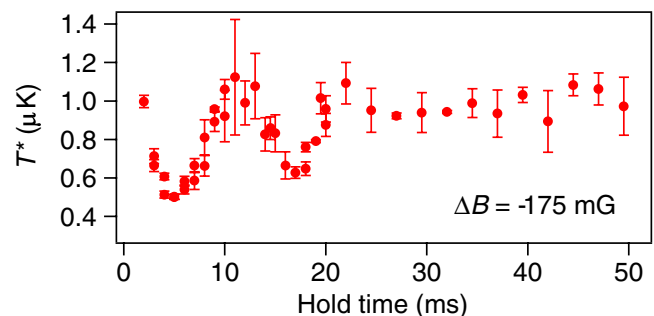

FIG. 3 (color online). Time evolution of T^*.

is evaluated to be 87(10) Hz, which agrees with twice the trap frequency of 39 Hz in the x direction. As seen in Fig. 3, $T^*(t)$ shows abrupt thermalization at $t = 20$ ms which we identify to be the thermalization time. It is reported that it takes about 2.7 collisions for the cloud to thermalize [30,31]. Based on this, the dimer-dimer elastic collision rate is estimated to be $(20 \text{ ms}/2.7)^{-1} \sim 140$ Hz.

We measured the lifetimes of molecules in all three combinations of $|1\rangle$ and $|2\rangle$ states. Figures 4(a)–4(c) show the numbers of $|1\rangle - |1\rangle$, $|1\rangle - |2\rangle$, and $|2\rangle - |2\rangle$ molecules remaining after the varying hold time at $\Delta B =$
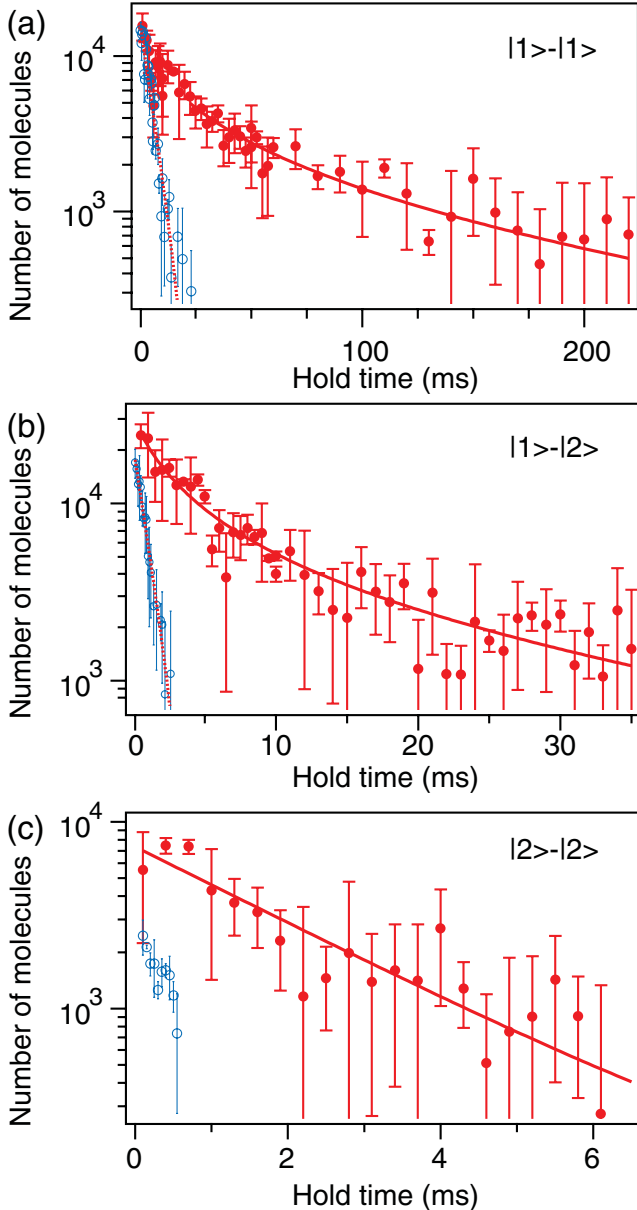

(a)

(b)

(c)

FIG. 4 (color).   Number of molecules vs hold time for $|1\rangle - |1\rangle$ (a), $|1\rangle - |2\rangle$ (b), and $|2\rangle - |2\rangle$ molecules (c). Solid circles show the decay data for molecules alone, and open circles show the decay data with both atoms and molecules present. The solid and dotted curves are the fittings for pure molecules and for atom-molecule mixtures.

-175 mG. In Fig. 4(a), the number of molecules is greater than that in Fig. 2(a) due to different experimental conditions. Solid circles show the number of molecules vs hold time under the condition that only molecules are held in the trap, and open circles show the same quantity in the presence of unpaired atoms. In the latter case, the blast light was turned on after the hold time to ensure that the signal arises exclusively from molecules. The molecular lifetime is greatly suppressed in the presence of unpaired atoms. The loss of molecules is analyzed according to the equation [27]

$$\frac{\dot{n}_d}{n_d} = -\alpha - K_{ad}n_a - K_{dd}n_d, \qquad (1)$$

where n_a and n_d are the density of atoms and that of molecules, α is the one-body decay rate of molecule, and K_{ad} and K_{dd} are the loss coefficients for atom-dimer and dimer-dimer inelastic collisions. In fitting Eq. (1) to experimental data, we use the peak densities of atoms and molecules for n_a and n_d. We assume that the spatial distribution of atoms obeys an ideal Fermi-Dirac distribution in a harmonic trap, and n_a is time independent since the number of atoms far exceeds that of molecules [32]. We also assume that the profile of molecules shows the Gaussian distribution and that the cloud size is time independent [27,29].

The measured decay rates are summarized in Table I. For $|1\rangle - |1\rangle$ molecules with no unpaired atoms, the decay curve is well fitted by Eq. (1) without the one-body decay term. As mentioned above, the molecular cloud undergoes breathing-mode oscillations, and the molecular density changes in time up to 20 ms. Therefore, we fit the decay to extract K_{dd} at $t \geq 20$ ms. For the $|1\rangle - |2\rangle$ molecules alone in the trap, we used the whole data for the fit. Since $|2\rangle$ is not the lowest energy state, $|1\rangle - |2\rangle$ molecules are expected to undergo dipolar decay into the lower spin state. Therefore, both α and K_{dd} contribute to the decay. With the initial density n_d, the decay rate $K_{dd}n_d$ is evaluated to be 390 Hz, which is 15 times larger than the one-body decay rate α. For $|2\rangle - |2\rangle$ molecules alone in the trap, an exponential decay fits the data well, indicating that the one-body decay is dominant. It is difficult to extract K_{ad} for $|2\rangle - |2\rangle$ molecules due to the low signal-to-noise ratio. Here, n_a is estimated to be 4.5, 8.0, and 4.5×10^{12} cm^{-3} for Figs. 4(a)–4(c). n_d is estimated to be 0.9, 4.8, and 1.1×10^{11} cm^{-3} for $|1\rangle - |1\rangle$ (at $t = 20$ ms), $|1\rangle - |2\rangle$ (at $t = 0$ ms), and $|2\rangle - |2\rangle$ (at $t = 0$ ms), respectively.

TABLE I.   One-body decay rate α, atom-dimer (K_{ad}) and dimer-dimer (K_{dd}) inelastic collision coefficients.

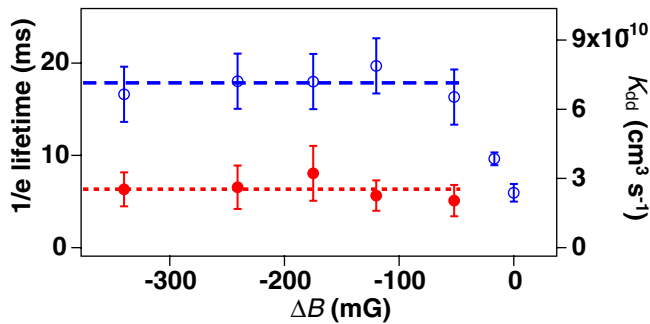|	$\alpha(s^{-1})$	$K_{ad}(10^{-11}$ cm^3 s$^{-1})$	$K_{dd}(10^{-10}$ cm^3 s$^{-1})$
$|1\rangle - |1\rangle$	0	$2.4^{+0.5}_{-0.3}$	2.8 ± 0.3
$|1\rangle - |2\rangle$	260 ± 150	$6.8^{+1.5}_{-1.1}$	8.1 ± 1.1
$|2\rangle - |2\rangle$	480 ± 60	$\cdots$	$\cdots$

FIG. 5 (color online). Lifetime (open circles) and dimer-dimer inelastic collision coefficient (solid circles) for $|1\rangle - |1\rangle$ molecules vs magnetic-field detuning. The dotted (dashed) lines show the averages of K_{dd} ($1/e$ lifetime) for $\Delta B < -50$ mG.

We measured the ΔB dependence of the $1/e$ lifetime and K_{dd} of the $|1\rangle - |1\rangle$ molecules (Fig. 5). For -340 mG $< \Delta B < -50$ mG, the lifetime is independent of ΔB and close to the thermalization time of 20 ms. Since the lifetime is expected to be shorter when $\Delta B > 0$ [20,21], our uncertainty in the resonance position could be as large as 50 mG. We evaluate and plot K_{dd} in Fig. 5 only in the range between -340 mG and -50 mG because neglecting the one-body decay term is justified only on the bound side of the resonance.

In conclusion, we have created $^6\text{Li}_2$ p-wave Feshbach molecules and studied their collisional properties. From the thermalization time of the breathing-mode oscillation, we evaluated the dimer-dimer elastic collision rate for $|1\rangle - |1\rangle$ molecules. From the decay of molecules, we obtained the dimer-dimer inelastic loss coefficients (for $|1\rangle - |1\rangle$ and $|1\rangle - |2\rangle$), the one-body decay coefficients (for $|1\rangle - |2\rangle$ and $|2\rangle - |2\rangle$), and the atom-dimer inelastic collision coefficients (for $|1\rangle - |1\rangle$ and $|1\rangle - |2\rangle$). We created 7×10^3 molecules at a temperature of 1 μK after thermalization. Provided molecules are distributed equally among three different m_l states, the phase space density is estimated to be 4×10^{-3}. With the initial molecular density of 2.1×10^{11} cm^{-3} and K_{dd} for $|1\rangle - |1\rangle$ molecules, our measurements show that the ratio of elastic to inelastic collision rate is about two, indicating that a conventional evaporative cooling is not an effective approach to achieve quantum degeneracy [33]. To overcome this, one could use a Feshbach resonance to enhance the dimer-dimer elastic collisions. One could also utilize the optical lattice to single out a specific m_l state [24] which should have a higher ratio of elastic to inelastic collision rates.

[1] C. A. Regal, M. Greiner, and D. S. Jin, Phys. Rev. Lett. **92**, 040403 (2004).
[2] M. W. Zwierlein *et al.*, Phys. Rev. Lett. **92**, 120403 (2004).
[3] T. Bourdel *et al.*, Phys. Rev. Lett. **93**, 050401 (2004).
[4] C. Chin *et al.*, Science **305**, 1128 (2004).
[5] J. Kinast *et al.*, Phys. Rev. Lett. **92**, 150402 (2004).
[6] G. B. Partridge *et al.*, Phys. Rev. Lett. **95**, 020404 (2005).
[7] L. You and M. Marinescu, Phys. Rev. A **60**, 2324 (1999).
[8] J. L. Bohn, Phys. Rev. A **61**, 053409 (2000).
[9] J. Levinsen, N. R. Cooper, and V. Gurarie, Phys. Rev. Lett. **99**, 210402 (2007).
[10] S. Botelho, and C. Sá de Melo, J. Low Temp. Phys. **140**, 409 (2005).
[11] Y. Ohashi, Phys. Rev. Lett. **94**, 050403 (2005).
[12] T.-L. Ho and R. B. Diener, Phys. Rev. Lett. **94**, 090402 (2005).
[13] V. Gurarie, L. Radzihovsky, and A. V. Andreev, Phys. Rev. Lett. **94**, 230403 (2005).
[14] C.-H. Cheng and S.-K. Yip, Phys. Rev. Lett. **95**, 070404 (2005).
[15] D. M. Lee, Rev. Mod. Phys. **69**, 645 (1997).
[16] Y. Maeno *et al.*, Nature (London) **372**, 532 (1994).
[17] J. Zhang *et al.*, Phys. Rev. A **70**, 030702(R) (2004).
[18] C. H. Schunck *et al.*, Phys. Rev. A **71**, 045601 (2005).
[19] J. Fuchs *et al.*, Phys. Rev. A **77**, 053616 (2008).
[20] J. P. Gaebler *et al.*, Phys. Rev. Lett. **98**, 200403 (2007).
[21] D. S. Jin, J. P. Gaebler, and J. T. Stewart, in *Proceedings of the International Conference on Laser Spectroscopy* (World Scientific, Telluride, Colorado, 2008).
[22] F. Chevy *et al.*, Phys. Rev. A **71**, 062710 (2005).
[23] C. A. Regal *et al.*, Phys. Rev. Lett. **90**, 053201 (2003).
[24] K. Günter *et al.*, Phys. Rev. Lett. **95**, 230401 (2005).
[25] K. Xu *et al.*, Phys. Rev. Lett. **91**, 210402 (2003).
[26] M. Mark *et al.*, Phys. Rev. A **76**, 042514 (2007).
[27] N. Syassen *et al.*, Phys. Rev. A **74**, 062706 (2006).
[28] The number of atoms remaining after the blast light is estimated to be lower than 6×10^2, which is the minimum number of atoms that can be detected in our imaging system.
[29] T. Mukaiyama *et al.*, Phys. Rev. Lett. **92**, 180402 (2004).
[30] C. R. Monroe *et al.*, Phys. Rev. Lett. **70**, 414 (1993).
[31] H. Wu and C. J. Foot, J. Phys. B **29**, L321 (1996).
[32] The effect of atomic loss is estimated and taken into account as errors of K_{ad} in Table I.
[33] W. Ketterle and N. J. van Druten, Adv. At. Mol. Opt. Phys. **37**, 181 (1996).